ADVANCED FUNCTIONAL MATERIALS
www.afm-journal.de

Lending Triarylphosphine Oxide to Phenanthroline: a Facile Approach to High-Performance Organic Small-Molecule Cathode Interfacial Material for Organic Photovoltaics utilizing Air-Stable Cathodes

Wan-Yi Tan, Rui Wang, Min Li, Gang Liu, Ping Chen, Xin-Chen Li, Shun-Mian Lu, Hugh Lu Zhu, Qi-Ming Peng, Xu-Hui Zhu, Wei Chen,* Wallace C. H. Choy,* Feng Li,* Junbiao Peng, and Yong Cao*

Dedicated to the 80th birthday of Prof. Xiao-Zeng You

Cathode interfacial material (CIM) is critical to improving the power conversion efficiency (PCE) and long-term stability of an organic photovoltaic cell that utilizes a high work function cathode. In this contribution, a novel CIM is reported through an effective and yet simple combination of triarylphosphine oxide with a 1,10-phenanthrolinyl unit. The resulting CIM possesses easy synthesis and purification, a high T_g of 116 °C and attractive electron-transport properties. The characterization of photovoltaic devices involving Ag or Al cathodes shows that this thermally deposited interlayer can considerably improve the PCE, due largely to a simultaneous increase in V_{oc} and *FF* relative to the reference devices without a CIM. Notably, a PCE of 7.51% is obtained for the CIM/Ag device utilizing the active layer PTB7:$PC_{71}BM$, which far exceeds that of the reference Ag device and compares well to that of the Ca/Al device. The PCE is further increased to 8.56% for the CIM/Al device (with J_{sc} = 16.81 mA cm^{-2}, V_{oc} = 0.75 V, *FF* = 0.68). Ultraviolet photoemission spectroscopy studies reveal that this promising CIM can significantly lower the work function of the Ag metal as well as ITO and HOPG, and facilitate electron extraction in OPV devices.

1. Introduction

Organic photovoltaic (OPV) cells have been the subject of current research interest due to light weight, mechanical flexibility and the potential to provide a low-cost solution for harvesting solar energy.[1,2] Among others, cathode interfacial material (CIM) which is placed between the active layer and cathode becomes a critical element in determining the power conversion efficiency (PCE) and durability of an OPV device.[3] As a result, introducing a proper CIM has been shown capable of producing multiple beneficial effects, including i) facilitating electron extraction in the presence of air-stable cathodes, ii) blocking exciton and hole transport to the cathode, and iii) preventing metal diffusion into the underlying active layer during thermal evaporation.

W.-Y. Tan, M. Li, G. Liu, Prof. X.-H. Zhu, Prof. J. B. Peng, Prof. Y. Cao
State Key Laboratory of Luminescent Materials and Devices (SKLLMD) and Institute of Polymer Optoelectronic Materials and Devices
South China University of Technology (SCUT)
Guangzhou 510640, China
E-mail: xuhuizhu@scut.edu.cn

R. Wang, Prof. W. Chen
Department of Physics
National University of Singapore
3 Science Drive 2
and Department of Chemistry
National University of Singapore
3 Science Drive 3
Singapore 117543
E-mail: phycw@nus.edu.sg

P. Chen, Q.-M. Peng, Prof. F. Li
State Key Laboratory of Supramolecular Structure and Materials
Jilin University, 2699
Qianjin Avenue, Changchun 130012, China
E-mail: lifeng01@jlu.edu.cn

X.-C. Li, S.-M. Lu, H. L. Zhu, Prof. W. C. H. Choy
Department of Electrical and Electronic Engineering
The University of Hong Kong
Pokfulam Road, Hong Kong, China
E-mail: chchoy@eee.hku.hk

DOI: 10.1002/adfm.201401685

The development of CIMs for organic photovoltaics is mainly based on several different lines, ranging from inorganic metal compounds such as halides and oxides[4] to organic small molecules[5,6] and conjugated[3a]/non-conjugated polymers.[7] Organic small-molecule based CIMs show a number of potentially attractive characteristics. They possess a well-defined chemical structure, ease of synthesis with high purity and low-temperature processability (via thermal evaporation).[1]

Bathocuproine (BCP) was the first organic compound as a cathode interfacial layer brought into an OPV cell.[8] Following this preliminary success, various attempts on organic molecular CIMs such as metal complexes,[9,10] substituted 1,10-phenanthrolines (BPhen[11] and DMPP,[12] pyridine derivatives,[13,14] 1,4,5,8-naphthalenetetracarboxylic dianhydride,[15] 1,3,5-tris(1-phenyl-1*H*-benzimidazol-2-yl)benzene[16] and zwitterions,[6b] have been reported in order to further improve the device PCE and/or stability. Consequently, based on these studies, a wide-band-gap CIM with a deep HOMO level, sufficient electron transport and morphological stability is favorable for OPV applications.

As a strong electron donor and acceptor, the rigid and planar chemical structure of 1,10-phenanthroline (Phen) is a versatile chelating agent and stabilizes in particular the low-valent metals.[17] However, BCP is mainly hampered by its tendency to crystallize with no detectable glass transition (T_c ≈186 °C, T_m ≈ 290 °C. See Figure S1 in the Supporting Information), while bathophenanthroline (BPhen)[8,11] shows a clear glass transition and yet a low T_g of ≈66 °C. Therefore, the design and development of morphologically robust CIMs based on Phen derivatives with preserved effective electron transport characteristic and simplified synthesis approaches to avoid potentially complicated and/or costly synthesis/purification methods commonly associated with the polypyridinyl compounds are highly desirable.

In this context, we report a novel cathode interfacial material **Phen-NaDPO** (**Scheme 1**). Introducing the polar bulky and chelating moiety (2-naphthyl)diphenylphosphine oxide (NaDPO) provides the resulting CIM with a high glass transition temperature (T_g ≈ 116 °C) and a high solubility in common low-polar and polar solvents. Moreover, analytically pure **Phen-NaDPO** is facilely available by column chromatography without sublimation. Noticeably, utilizing a thermally deposited **Phen-NaDPO** interlayer provided the photovoltaic device that contained the active layer PTB7:$PC_{71}BM$ and Ag cathode with a 7.51% of PCE, which far surpasses the reference Ag device devoid of a CIM and even compares well with that of the Ca/Al device. In situ ultraviolet photoelectron spectroscopy (UPS) and X-ray photoelectron spectroscopy (XPS) measurements were used to reveal the working mechanism of this new CIM in terms of the interfacial energy level alignment. While **Phen-NaDPO** on graphite (HOPG) and ITO possesses low work function of around 3.0 eV, its strong chelating interaction with Ag surface may account for the further reduced work function as low as 2.6 eV on the metal cathode. The PCE was further increased from 7.51 to 8.56% for the **Phen-NaDPO**/Al device.

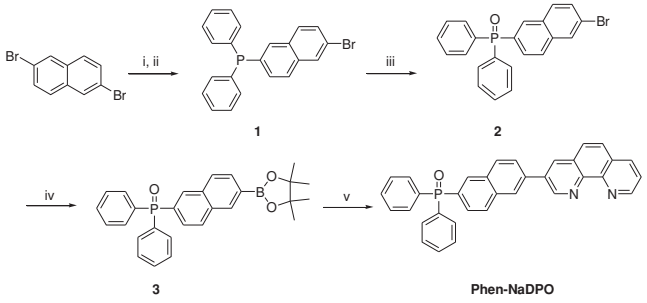

Scheme 1. Synthetic route to **Phen-NaDPO:** i) *n*-BuLi, THF, –78 °C; ii) chlorodiphenylphosphine; iii) H_2O_2, dichloromethane, room temperature; iv) Pd(dppf)Cl_2, KOAc, DMF, 80 °C; v) Pd$(OAc)_2$, tricyclohexylphosphine, 2 M K_2CO_3 aqueous solution, toluene, ethanol, 90 °C.

2. Results and Discussion

2.1. Synthesis of Phen-NaDPO

The synthesis of **Phen-NaDPO** is outlined in Scheme 1. Monolithiating 2,6-dibromonaphthalene, followed by treatment of chlorodiphenylphosphine leads to the monobromo compound **1**, which further gives compound **2** under oxidation with an excessive of H_2O_2 (Scheme 1). Subsequently, the successful boronation of compound **2** using bis(pinacolato) diboron provides the key precursor compound **3**. Finally **Phen-NaDPO** is obtained by Suzuki coupling of compound **3** and 3-bromo-1,10-phenanthroline.

The identity and purity of **Phen-NaDPO** are confirmed by ^{1}H NMR, HRMS and microanalysis (See Figure S2). It is worth noting that analytically pure compound can be facilely available through purification based mainly on column chromatography without further sublimation. This demonstrates the great advantage over the commonly used electron-transporting CIMs based on polypyridinyl derivatives, which usually involves extra sublimation purification steps with high cost.

In addition to a high solubility in low-polar solvents such as CH_2Cl_2, attaching this particular triarylphosphine oxide moiety to 3-position of 1,10-phenanthroline produces an increase of solubility in common alcohol solvents, relative to BCP and BPhen. For instance, 10 mg of **Phen-NaDPO** can be easily solubilized in 1 mL isopropanol (IPA) at room temperature.

2.2. Thermal and Morphological Properties of Phen-NaDPO

Phen-NaDPO shows a high thermal stability over 350 °C (**Figure 1**a). Although it first melted at 250 °C, no crystallization upon cooling or remelting was observed. Instead, an obvious glass transition emerged at approximately 116 °C during the cooling and reheating processes (Figure 1b), which is considerably higher than that of Bphen (T_g ≈ 66 °C) and TmPyPB (T_g ≈ 79 °C), a widely used electron-transporting layer in organic light-emitting diodes and more recently as a CIM in OPV device,[13b,c] whereas no detectable glass transfixion is present for BCP, apart from melting and crystallization (See Figure S1, Supporting Information). The stable amorphous morphology of **Phen-NaDPO** with a small surface roughness (R_{rms} = 0.622 nm) was further witnessed by the atomic force microscopy (AFM) measurement of the thermally deposited thin film (180 nm), annealed at 100 °C for 10 min (Figure 1c).

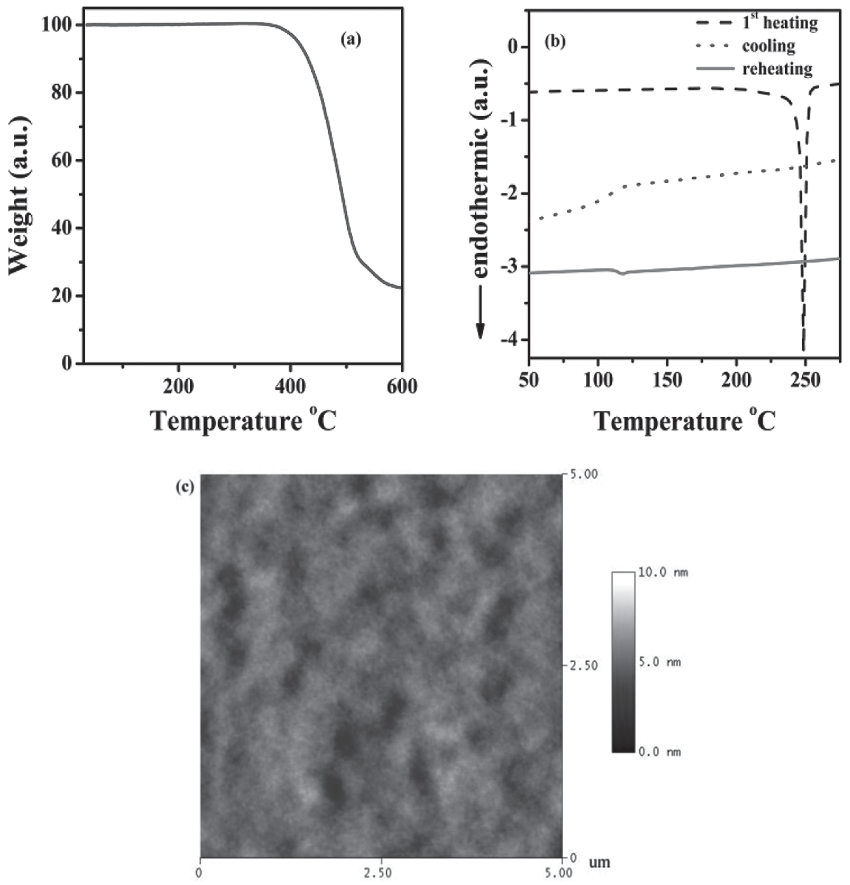

Figure 1. a) Thermogravimetric analysis, b) DSC diagrams, and c) Topographic AFM images of the thermally evaporated thin film (180 nm) of **Phen-NaDPO**, annealed at 100 °C for 10 min.

2.3. Phen-NaDPO as a Cathode Interfacial Layer in OPV Devices

Phen-NaDPO was first evaluated by thermal deposition as a cathode interfacial layer in photovoltaic devices (ITO/PEDOT:PSS/P3HT:$PC_{61}BM$/CIM(3–15 nm)/cathode). The Ag and Al metals were used as the cathodes, respectively. The analogue devices utilizing metal-only (Ag or Al) or Ca/Al as the cathode without CIM were also fabricated for comparison.

Inserting a thin layer of **Phen-NaDPO** (5 nm) led to a largely improved photovoltaic performance relative to the corresponding reference Ag device (**Figure 2**a and **Table 1**) with J_{sc} = 8.56 mA cm^{-2}, V_{oc} = 0.61 V, FF = 0.69 and PCE = 3.61%, which is comparable to those of the analogue devices utilizing a conjugated polymer electrolyte[18a] or self-assembled ammonium salt layer.[18b] By contrast, the reference Ag device without this interlayer gave a PCE of 2.18% with J_{sc} = 9.72 mA cm^{-2}, V_{oc} = 0.48 V, FF = 0.47.

Replacing the active layer with the PTB7:$PC_{71}BM$ blend[19] in the presence of **Phen-NaDPO** produced a further increase of PCE to 7.51% (J_{sc} = 18.04 mA cm^{-2}, V_{oc} = 0.71 V, FF = 0.59), whereas the reference Ag device showed an invariably considerably lower PCE of ≈2.19% with J_{sc} = 16.46 mA cm^{-2}, V_{oc} = 0.38 V, FF = 0.35 (**Figure 3**a and **Table 2**). Notably, the experimental J_{sc} values agreed well with those calculated from the incident photon-to-current efficiency (IPCE) measurement within 300–800 nm (See Figure S3 and Table S1 in the Supporting Information).

V_{oc} is influenced by the electrical contact between the active layer and the electrodes, as well as the HOMO level of the donor and LUMO level of the acceptor.[20,21] Similar to the **Phen-NaDPO**/Al and Ca/Al devices (as discussed below, Figure 2b, 3c and Table 1,2), introducing a **Phen-NaDPO** interlayer provides a V_{oc} of ≈0.60 V concerning the active layer P3HT:$PC_{61}BM$ and ≈0.70 V concerning PTB7:$PC_{71}BM$ for the Ag cathode, indicating an Ohmic contact between the active layer and the interfacial layer on the metal cathodes.

The high FF of the photovoltaic devices that contained a **Phen-NaDPO** interlayer can be understood in terms of the series resistance (R_s) and the shunt resistance (R_{sh}), which are calculated from the inverse slope near V_{oc} and V = 0 V in the photocurrent density–voltage curves, respectively.[21] The resulting generally smaller R_s and higher R_{sh} values, as compared to those of the reference devices without a CIM, reveal that **Phen-NaDPO** can effectively reduce the contact resistance between $PC_{61}BM$ and the Ag cathode.

Furthermore the **Phen-NaDPO**/Ag device showed a far better diode characteristic than the reference Ag device in the dark with a rectification ratio of ≈3.7×10^4 versus 9.6×10^2 at ±2 V (Figure 3b). This observation implies that **Phen-NaDPO** can effectively block hole injection while meanwhile improving

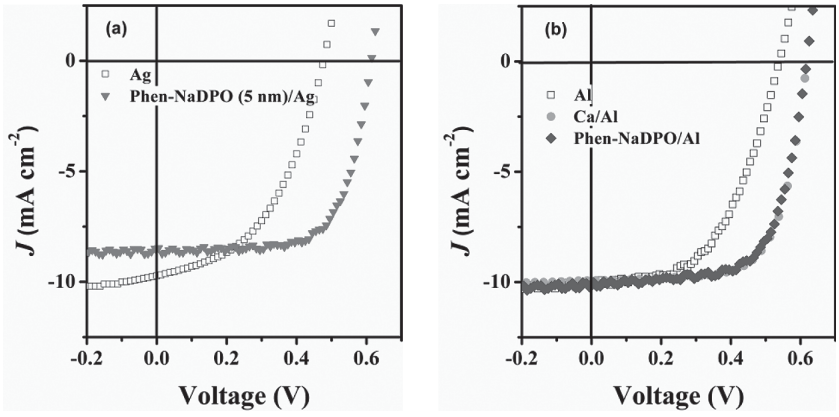

Figure 2. *J–V* characteristics of the photovoltaic devices (ITO/PEDOT:PSS/P3HT:$PC_{61}BM$/CIM(*x* nm)/cathode). *x* = 5 nm for **Phen-NaDPO**/Ag, 3 nm for **Phen-NaDPO**/Al and 0 nm for the reference Ag, Al, and Ca/Al devices.

Table 1. Summary of the photovoltaic data (ITO/PEDOT:PSS/P3HT:$PC_{61}BM$/CIM(*x* nm)/cathode), under light intensity of 100 mW cm^{-2}. Cathode = Ag, Al and Ca/Al.

CIM/Cathode	CIM [nm]	PCE [%]	J_{sc} [mA cm^{-2}]	V_{oc} [V]	FF	R_s [Ω cm^2]	R_{sh} [KΩ cm^2]
Ag	0	2.18(2.10)	9.72(9.77)	0.48(0.48)	0.47(0.45)	10.60	0.29
Phen-NaDPO/Ag	3	2.84(2.80)	8.57(8.74)	0.60(0.60)	0.55(0.54)	12.88	0.48
	5	3.61(3.59)	8.56(8.53)	0.61(0.61)	0.69(0.69)	5.75	0.96
	10	3.37(3.39)	9.29(9.53)	0.59(0.60)	0.61(0.60)	7.20	0.75
	15	3.42(3.20)	8.49(7.95)	0.61(0.61)	0.67(0.66)	9.05	2.56
Al	0	2.84(2.82)	10.06(10.09)	0.54(0.53)	0.53(0.52)	13.06	0.73
Ca/Al	0	4.18(4.01)	9.93(9.42)	0.61(0.61)	0.69(0.69)	2.93	4.32
Phen-NaDPO/Al	3	4.14(4.07)	10.23(10.10)	0.61(0.61)	0.66(0.66)	5.47	0.96
	5	4.04(3.96)	9.64(9.57)	0.62(0.61)	0.68(0.67)	5.05	0.69
	10	4.06(3.98)	9.95(9.75)	0.61(0.61)	0.67(0.67)	5.12	0.98
	15	3.63(3.59)	9.58(9.19)	0.61(0.61)	0.62(0.64)	10.14	1.45

The data in parentheses are the average results of three devices.

electron injection over a voltage of ≈0.4 V in the forward direction.

2.4. Photoelectron Spectroscopy Measurements

In order to get an in-depth understanding of the effects of the present CIM **Phen-NaDPO** on electron extraction in OPV devices, the interfacial electronic structures of **Phen-NaDPO** on various substrates were systematically evaluated by UPS in **Figure 4**. The UPS spectra at the low kinetic energy region (Figure 4a) reveal the evolution of vacuum level and hence the surface work function of Ag substrate upon the deposition of CIM. A tremendous vacuum level downward shift of 1.98 eV can be observed after the deposition of 10 nm **Phen-NaDPO** film on Ag, with the work function of Ag reduced to 2.64 eV. Such low work function can greatly facilitate the electron extraction in OPVs.

From the UPS spectra near the Fermi level region (Figure 4b), the HOMO edges for **Phen-NaDPO** films on Ag locate at the binding energy of 3.30 eV below the Fermi level for 10 nm thickness. The optical band gap of **Phen-NaDPO** was measured to be 3.36 eV (See Figure S4, Supporting Information). Due to the large exciton binding energy in organic materials, the HOMO-LUMO electronic band gap is usually a few hundred meV larger than the optical band gap. Combining with the deep lying HOMO levels, the LUMO of **Phen-NaDPO** can be deduced to locate right above the Fermi level, thereby facilitating electron transfer during the electron extraction via these low-lying LUMO states of the CIM. The evolution of thickness-dependent XPS core level spectra in Figure S5 reveals the existence of strong interaction at the interface between **Phen-NaDPO** film and Ag (while not existent between CIM and HOPG), apparently via

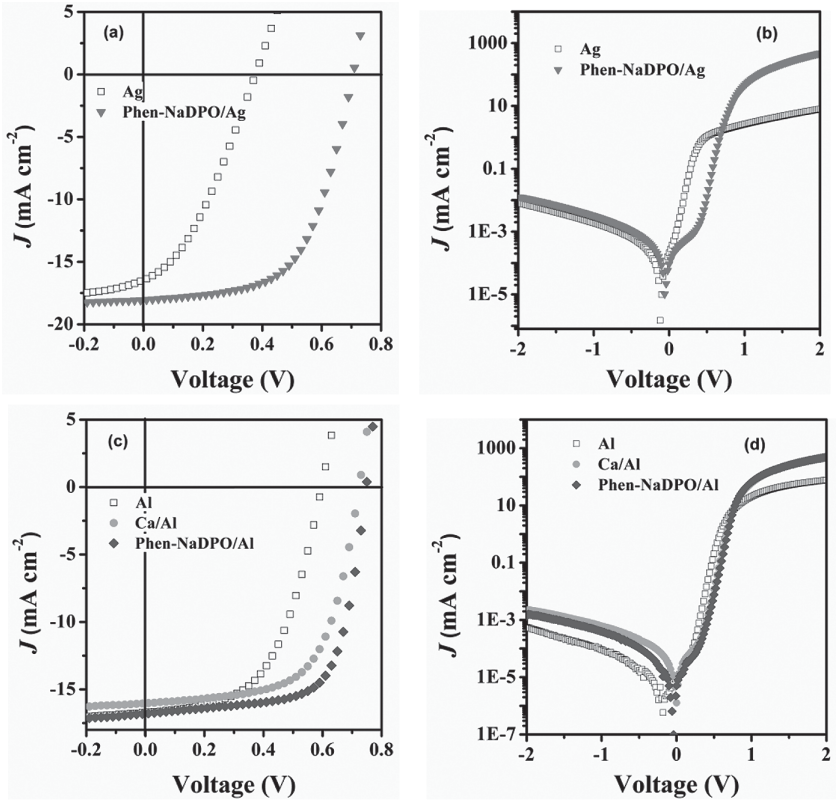

Figure 3. a,c) Light and b,d) dark *J–V* characteristics of the photovoltaic devices (ITO/PEDOT:PSS/PTB7:$PC_{71}BM$/CIM(*x* nm)/cathode). *x* = 3 nm for **Phen-NaDPO/**Ag or Al, and 0 nm for the reference Ag, Al and Ca/Al devices. The active layer was spin-cast from a mixture of chlorobenzene and DIO (100:3 V/V).

Table 2. Summary of the photovoltaic data (ITO/PEDOT:PSS/PTB7:$PC_{71}BM$/CIM(x nm)/cathode), under light intensity of 100 mW cm^{-2}. Cathode = Ag, Al and Ca/Al.

CIM/Cathode	CIM [nm]	PCE [%]	J_{sc} [mA cm^{-2}]	V_{oc} [V]	FF	R_s [Ω cm^2]	R_{sh} [KΩ cm^2]
Ag	0	2.19(2.12)	16.46(16.43)	0.38(0.37)	0.35(0.35)	14.82	0.14
Phen-NaDPO/Ag	3	7.51(7.44)	18.04(18.04)	0.71(0.70)	0.59(0.59)	4.40	0.76
Al	0	5.43(5.37)	16.69(16.66)	0.60(0.60)	0.54(0.54)	7.94	0.55
Ca/Al	0	7.31(7.26)	16.04(16.21)	0.72(0.72)	0.63(0.62)	4.54	0.65
Phen-NaDPO/Al	3	8.56(8.37)	16.81(16.72)	0.75(0.74)	0.68(0.67)	3.61	0.49

The data in parentheses are the average results of three devices.

the coupling between the P = O functional group with Ag. Furthermore the rigid phenanthrolinyl moiety has been shown to interact with various metals including Al and Ag.[17,22] Such strong interactions can promote a good electrical contact between the CIM and Ag electrodes.

On inert substrate of graphite (e.g., HOPG) and the widely used ITO substrate, the coating of **Phen-NaDPO** film can also lead to the significant reduction on surface work function, i.e., the surface work function can be reduced to 3.02 eV (**Phen-NaDPO** on HOPG), and 3.10 eV (**Phen-NaDPO** on ITO), respectively, as shown in Figure 4. This observation suggests that **Phen-NaDPO** film can be used as a potentially universal low work function surface modification layers on various substrates.

We further evaluate the interface between the low work function CIM and the active acceptor molecules (*n*-type) by using C_{60} as a model system. As shown in **Figure 5**a, during the sequential deposition of C_{60} on **Phen-NaDPO** modified ITO substrate, the vacuum level was gradually upward shifted, or the work function was increased by 1.16 eV. This was accompanied by an obvious upward band-bending like behavior in C_{60} film, that is, the HOMO of C_{60} moved towards the Fermi level

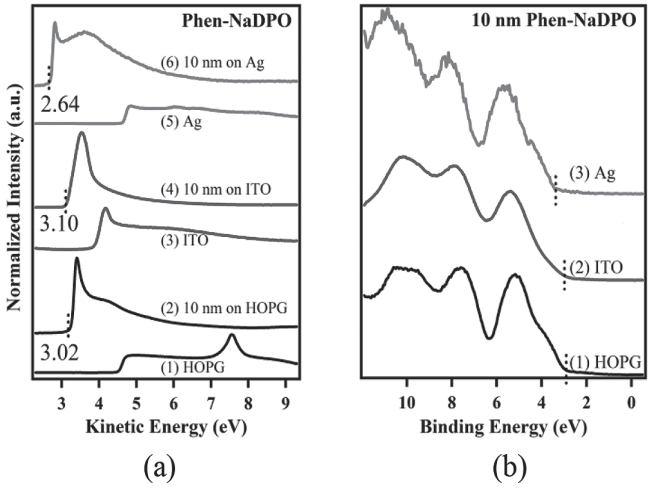

Figure 4. UPS spectra at a) the low-kinetic energy part and b) valence band spectra near the Fermi level for 10 nm **Phen-NaDPO** on Ag, ITO, and HOPG surface. The work function of pristine substrates was also provided in (a).

(Figure 5b). Based on such observation, the low work function of the present **CIM** can induce significant electron transfer from the substrate via **CIM** film to C_{60}, leading to the notable increase of work function (Figure 5c) and the formation of a large interfacial dipole or the build-in electric field (Figure 5d). By contrast, the charge transfer between the unmodified ITO and C_{60} appears negligible.[23] As a result, the LUMO level of C_{60} is situated right above the Fermi level at the interface (Figure 5c), thereby facilitating the effective electron extraction from organic acceptor through the **Phen-NaDPO** interface layer (via the low-lying LUMO) to the cathode electrode, as well as minimizing the energy loss during the electron extraction process. Moreover, the build-in electric field in favorable direction can greatly facilitate electron extraction from the active layer to the cathode (Figure 5d).

2.5. Photovoltaic Devices Based on Phen-NaDPO/Al Cathode

It is expected that **Phen-NaDPO** should be also effective for the Al cathode. As a result, the photovoltaic device concerning the active layer P3HT:$PC_{61}BM$ and Al cathode in the presence of the **Phen-NaDPO** interlayer (≈3 nm) yielded an increase of PCE to 4.14% with J_{sc} = 10.23 mA cm^{-2}, V_{oc} = 0.61 V, FF = 0.66, which is comparable to that of the Ca/Al device (Figure 2b and Table 1). By contrast, the reference Al cathode without a CIM gives a PCE of 2.84% with J_{sc} = 10.06 mA cm^{-2}, V_{oc} = 0.54 V,[18] FF = 0.53.

Further, a high PCE of 8.56% was obtained for the **Phen-NaDPO**/Al device based on the active layer PTB7:$PC_{61}BM$ with J_{sc} = 16.81 mA cm^{-2}, V_{oc} = 0.75 V, FF = 0.68, which surpassed that of 5.43% of the reference Al and even 7.31% of the Ca/Al devices (Figure 3c and Table 2). Notably, very similar PCEs were found at both SKLLMD, South China University of Technology and the University of Hong Kong to demonstrate reproducibility. The PCE is also comparable to those of the analogue devices achieved by utilizing a conjugated polymer interlayer.[24]

The photovoltaic devices that consisted of a **Phen-NaDPO** interlayer appear to provide a slow decrease of PCE with the increasing thickness (Table 1 and Supporting Information Figure S6). For instance, as the interlayer thickness reached 15 nm, the PCE still remained at 3.42% for the **Phen-NaDPO**/Ag device and 3.63% for the **Phen-NaDPO**/Al device. Generally, a thicker CIM is beneficial to large area device processing,

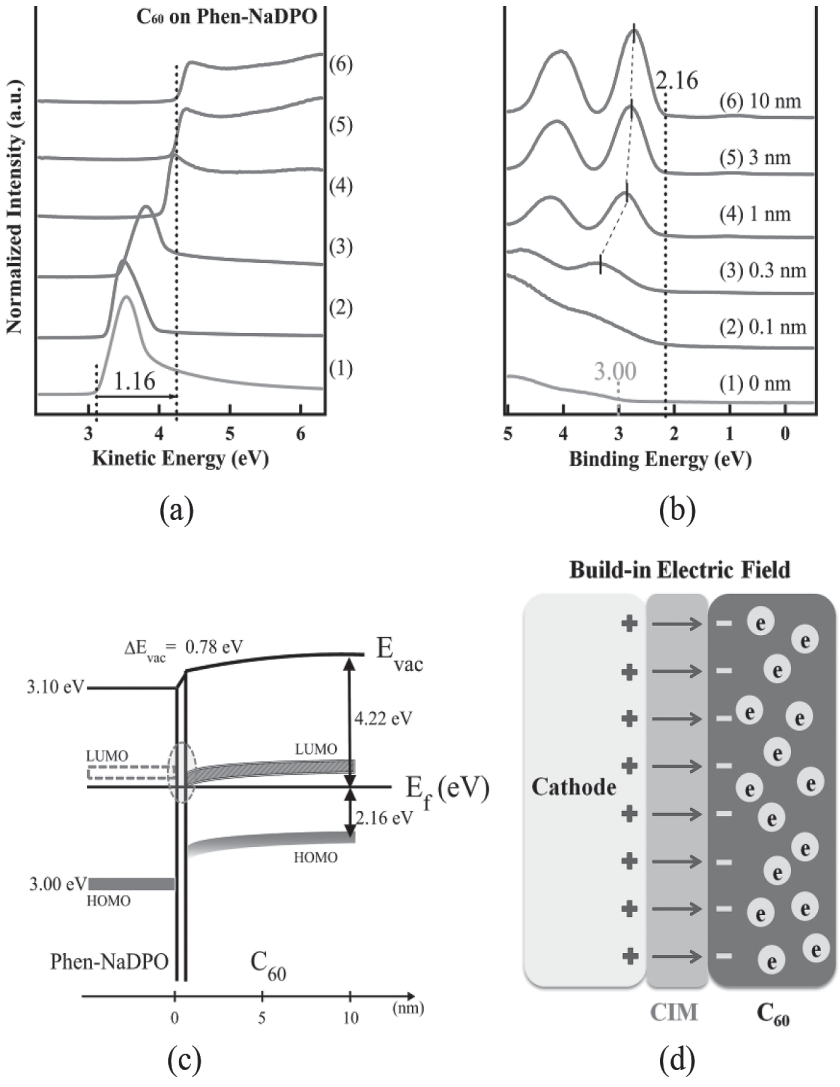

Figure 5. Thickness-dependent UPS spectra at a) the low-kinetic energy part, b) low binding energy part near the Fermi level, c) the schematic energy diagram of C_{60} on **Phen-NaDPO** as a function of C_{60} thickness, and d) the schematic of the additional electrical field formed by inserting CIM.

while certain CIMs based on inorganic and organic salts such as LiF[4a] and zwitterions[6b] are effective within only a few angstroms to nanometers.

2.6. Electron-Transport Property of Phen-NaDPO

The electron transport property of **Phen-NaDPO** was preliminarily evaluated by the time-of-flight (TOF) technique with a device configuration (ITO/Alq_3(20 nm)/**Phen-NaDPO**(1.5 μm)/Al). Tris(8-hydroxyquinolinato)Luminal (Alq_3) was used as the charge-generation layer (CGL). A typical double logarithmic plot of TOF transient photocurrent at $E = 1.1 \times 10^6$ V cm^{-1} was shown in **Figure 6**. The transit time of electrons was 0.4 μs, yielding an electron mobility of 3.3×10^{-4} cm^2 V^{-1} s^{-1}, which is comparable to that of BPhen.[25] Nevertheless, the electron mobility of **Phen-NaDPO** tends to increase at low electric fields, amounting to 3.9×10^{-4} cm^2 V^{-1} s^{-1} at E = ~8×10^5 V cm^{-1} (See the inset of Figure 6).

2.7. Phen-NaDPO vs NaBDPO as a CIM for OPV Devices

Finally it is worth noting that **Phen-NaDPO** generally provides a better photovoltaic performance than (naphth-2,6-diyl) bis(diphenylphosphine oxide) (**NaBDPO**, Figure S7, S8 and Table S2, Supporting Information), especially for the Ag cathode. The cathode interfacial materials based on diphenylphosphine oxide(s) have been shown effective for the Al cathodes.[18c]

3. Conclusions

In summary, lending the triarylphosphine oxide moiety to 1,10-phenanthroline provides the present CIM with multiple attractive characteristics such as easy accessibility and purification, a high T_g of 116 °C, and good electron transport properties. The photovoltaic devices that contained a thermally deposited **Phen-NaDPO** interlayer and Ag or Al cathode produced a considerably improved PCE, due largely to a simultaneous increase in V_{oc} and FF relative to the reference devices without a CIM. Notably, a PCE of 7.51% was obtained for the **Phen-NaDPO**/Ag device utilizing the active layer PTB7:$PC_{71}BM$, which far exceeds that of the reference Ag device and even compares well to that of the Ca/Al device. The PCE was further increased to 8.56% for the **Phen-NaDPO**/Al device (with J_{sc} = 16.81 mA cm^{-2}, V_{oc} = 0.75 V, FF = 0.68). In situ UPS and XPS experiments were carried out to explain the functions of **Phen-NaDPO** in the OPV devices based on the energy level alignments at the CIM/metal and C_{60}/CIM interfaces. **Phen-NaDPO** on Ag possessed a low work function of 2.64 eV to facilitate effective electron extraction in OPV devices. It is found that **Phen-NaDPO** can also work as a universal and effective cathode interfacial material for various substrates including ITO and HOPG. While the photovoltaic polymers were employed to facilitate the characterization of **Phen-NaDPO** as a cathode interfacial layer, it is expected that the present CIM may afford promising small-molecular OPV devices in both conventional and inverted device configurations through vacuum thermal deposition. Moreover, the findings reported here may stimulate further intensive interest in this kind of small-molecule CIMs for organic optoelectronics.

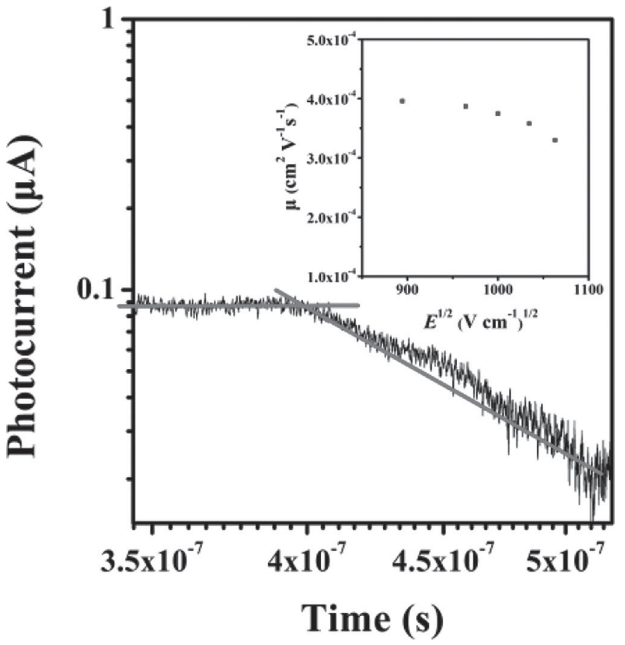

Figure 6. Typical double logarithmic plot of TOF transient photocurrent of electrons of **Phen-NaDPO** at $E = 1.1 \times 10^6$ V cm^{-1}, showing a clear "plateau" region. The insert: electron mobilities vs $E^{1/2}$.

4. Experimental Section

All manipulations involving air-sensitive reagents were performed under dry nitrogen. Tetrahydrofuran (THF) was dried with molecular sieves (3 Å). All other starting materials were purchased commercially and used as received, unless otherwise specified.

Synthesis of (2-bromo-naphth-6-yl)diphenylphosphine oxide (Compound 2): A solution of 2,6-dibromonaphthalene (3 g, 10.5 mmol) in anhydrous THF (180 mL) was degassed under N_2 for 30 min, and then cooled to –78 °C. *n*-Butyllithium (2.4 M solution in hexane, 4.8 mL, 11.55 mmol) was added dropwise via syringe. The solution continued to be stirred for 40 min, and then chlorodiphenylphosphine (2.3 mL, 12.6 mmol) was then added via syringe. The reaction mixture was stirred overnight whilst gradually warming to room temperature. Upon concentration, the residue was treated with water and extracted by CH_2Cl_2. The organic layer was separated, dried over anhydrous $MgSO_4$, filtered and concentrated under reduced pressure. The residue was subject to column chromatography over silica gel using petroleum ether/CH_2Cl_2 (v/v = 5/1) as the elute to afford 2-bromo-6-diphenylphos-phinonaphthalene (**Compound 1**) as a white solid, which was used directly for oxidation. Hydrogen peroxide (30%, 10 mL) was then added to a stirred mixture of compound **1** in CH_2Cl_2 (30 mL). The reaction stirred at room temperature overnight. The mixture was treated with aqueous $NaHSO_3$ (2 M) and then extracted with CH_2Cl_2. The organic layer was separated, dried over anhydrous $MgSO_4$, filtered and concentrated under reduced pressure. Yield: 3.3 g (78%). ^{1}H NMR (300 MHz, DMSO, ppm, δ): 7.53–7.60 (m, 4H), 7.62–7.77 (m, 8H), 8.03–8.08 (m, 2H), 8.33 (s, 1H), 8.36 (d, 1H, J = 13.9 Hz).

Synthesis of (2-(4,4,5,5-tetramethyl-1,3,2-dioxaborolan-2-yl)naphth-6-yl) diphenylphosphine oxide (Compound 3): Pd(dppf)Cl_2 (81 mg, 0.11 mmol) was added to a mixture of aqueous KOAc (977 mg, 9.95 mmol), compound **2** (1.35 g, 3.32 mmol), and 4,4,5,5-tetramethyl-2-(4,4,5,5-tetramethyl-1,3,2-dioxaborolan-2-yl)-1,3,2-dioxaborolane (1.26 g, 4.98 mmol) in 1,4-dioxane (30 mL) under N_2. The reaction was heated at 80 °C for 2 h. After being cooled to room temperature, distilled water was added. The organic layer was extracted with CH_2Cl_2, separated, dried over anhydrous $MgSO_4$, filtered and concentrated under reduced pressure. The crude product was subject to column chromatography over silica gel using CH_2Cl_2/ethyl acetate (v/v = 3/1) as the elute to afford a white solid. Yield: 2.8 g (60%). (300 MHz, DMSO, ppm, δ): 1.34 (s, 12H), 7.53–7.71 (m, 11H), 7.79 (d, 1H, J = 8.2 Hz), 8.05 (d, 1H, J = 8.4 Hz), 8.16 (d, 1H, J = 13.7 Hz), 8.39 (s, 1H).

Synthesis of (2-(1,10-phenanthrolin-3-yl)naphth-6-yl)diphenylphosphine oxide (**Phen-NaDPO**): $Pd(OAc)_2$ (4.5 mg, 0.02 mmol) and tricyclohexylphosphine (11.2 mg, 0.04 mmol) was added to a mixture of aqueous K_2CO_3 (2 M, 2 mL, 4 mmol), compound **3** (289 mg, 0.64 mmol), and 3-bromo-1,10-phenanthroline (150 mg, 0.58 mmol) in toluene (30 mL) and ethanol (4 mL) under N_2. The reaction was heated at 90 °C overnight. After being cooled to room temperature, the mixture was extracted with CH_2Cl_2. The organic layer was separated, dried over anhydrous $MgSO_4$, filtered and concentrated under reduced pressure. The crude product was subject to column chromatography over silica gel using CH_2Cl_2/ethanol (v/v = 50/1) as the elute to afford a white solid. Yield: 200 mg (68%). m. p.: 250 °C (in the 1st heating run). T_g: 116 °C (in the 2nd heating run). ^{1}H NMR (300 MHz, DMSO, ppm, δ): 7.56–7.81 (m, 12H), 8.04–8.12 (m, 2H), 8.21–8.31 (m, 3H), 8.44 (d, 1H, J = 13.5 Hz), 8.53 (dd, 1H, J = 8.1, 1.7 Hz), 8.67 (s, 1H), 8.99 (s, 1H), 9.14 (dd, 1H, J = 4.3, 1.7 Hz), 9.62 (s, 1H). HRMS (ESI) m/z: $[M + H]^+$ calcd. for $C_{34}H_{24}N_2OP$, 507.1626; found, 507.1630. Anal. calcd. For $C_{34}H_{23}N_2OP$: C 80.62, H 4.58, N, 5.53. Found: C 80.38, H 4.57, N 5.54.

Surface and Interface Analysis: In situ UPS and XPS measurement were carried out in a custom designed ultrahigh vacuum (UHV) system with a base pressure better than 2×10^{-10} mbar. A helium discharge UV lamp with energy of 21.2 eV (He I) was used as the source of UV light. XPS was performed with the Al Kα line with a photo energy of 1486.6 eV. All data was recorded by the Omicron EA 125 hemisperical analyzer at normal emission angle under room temperature. Vacuum level was determined from UPS spectra at the low-kinetic energy onset (secondary electron cut-off) with –5 V sample bias. The work function of the substrate Φ was obtained through the equation $\Phi = h\nu - W$, where W is the spectrum width of the energy difference between substrate Fermi level and secondary electron cutoff. The plots in the UPS kinetic energy figures were offset by 0.7 eV to view the value of the sample work function directly. The CIM and C_{60} were thermally evaporated from separated Knudsen cells onto the substrates in an UHV preparing chamber with a base pressure better than 3×10^{-9} mbar. The deposition rate and hence the "nominal" thickness were in situ monitored by Quartz crystal microbalance during deposition and further calibrated by XPS by monitoring the peak intensity attenuation of the substrate core level peaks. The Ag(111) substrate was cleaned by several cycles of Ar^+ ion sputtering and subsequently annealed at 800 K. Freshly cleaved HOPG was degassed in UHV chamber at around 600 K overnight before deposition. ITO substrates were cleaned by subsequent sonication in acetone, isopropyl alcohol and deionized water before loaded to the chamber.

Fabrication and Characterization of Photovoltaic Devices: ITO-coated glass substrates were cleaned by sonication in acetone, detergent, deionized water, and isopropyl alcohol and dried in a nitrogen stream, followed by an oxygen plasma treatment. In order to fabricate photovoltaic devices, a thin hole-collection layer (ca. 40 nm) of PEDOT:PSS (Baytron PVPAI 4083, filtered at 0.45 μm) was spin-cast on the pre-cleaned ITO-coated glass substrates and baked at 120 °C for 20 min under ambient conditions. The active layer P3HT:$PC_{61}BM$ was prepared by spin-casting 1,2-dichlorobenzene solution (20:20 mg mL^{-1}) at 800 rpm for 36 s in a dry box, dried in covered glass Petri dishes at room temperature for 30 min, and thermally annealed at 110 °C for 10 min. The active layer PTB7:$PC_{71}BM$ (10:15 mg mL^{-1}) was prepared by spin-casting chlorobenzene solution with the addition of a small amount of DIO (CB:DIO = 100:3, V/V) at 1500 rpm for 30 s in dry box. The thickness of the PTB7:$PC_{71}BM$ layer was about 100 nm. **Phen-NaDPO** and **NaBDPO** were either deposited by thermal evaporation at 0.2 Å s^{-1} in vacuum ($<5 \times 10^{-4}$ Pa or spin-cast atop the active layer from IPA solution with the same concentration of 0.5 mg mL^{-1} at 2000 rpm. The Al and Ag electrode were thermally deposited for 100 nm and 60 nm, respectively, through a mask in vacuum ($<5 \times 10^{-4}$ Pa). All steps except processing of PEDOT:PSS were performed in the glove box. The effective device area was about 0.04 cm^2 for the active layer P3HT:$PC_{61}BM$ and 0.06 cm^2 for PTB7:$PC_{71}BM$. The current density–voltage (J–V) characteristics were

measured using a Keithley 2400 source meter. The photovoltaic devices were characterized using a calibrated AM1.5 G solar simulator (Oriel model 91192), under light intensity of 100 mW cm^{-2}.

Mobility Measurements using the Time-of-Flight (TOF) Technique: Device configuration (ITO/Alq_3/**Phen-NaDPO**/Al). Alq_3 (20 nm) and **Phen-NaDPO** (1.5 μm) were deposited by thermal evaporation in vacuum (< 6×10^{-4} Pa) at a rate of 0.2 and 3 Å s^{-1}, respectively. The Al electrode (15 nm) were thermally deposited through a mask. The effective device area was about 0.04 cm^2. A Nd:YAG laser ($\lambda = 355$ nm, pulse width: 5 ns) was used as the light source and Alq_3 as the charge-generation layer (CGL). The applied voltage was controlled by a Keithley 2400 source meter. The electrons moved toward the Al contact with a negative voltage. The photocurrent was characterized across the load resistor using a digital storage oscilloscope (DPO7104, bandwidth: 1 GHz). The electron mobility was deduced from

$$\mu = \frac{d}{\tau E} \quad (1)$$

where d is the thickness of **Phen-NaDPO**, τ the transit time of electrons, and E the electric field.

Supporting Information

Supporting Information is available from the Wiley Online Library or from the author.

Acknowledgments

W.Y.T. and R.W. contributed equally to this work. X.H.Z. is grateful for the financial support of SCUT, NSFC, and MOST of China (Grant Nos. 2014CB643500, 2014ZG0009, 51173051, U1301243, and 91333206). W.C. acknowledges the financial support from Singapore MOE Grants R143–000–505–112, R143–000–530–112, R143–000–542–112 and R143–000–559–112. W.C.H.C. would like to acknowledge the financial support of the Research Grants Council (RGC) of Hong Kong Special Administrative Region for the General Research Fund (grants: HKU711813 and HKU711612E), the RGC-NSFC grant (N-HKU709/12) and the ERG-SRFDP grant (M-HKU703/12). The authors are thankful to Prof. Wei-Hong Zhu at East China University of Science and Technology for the generous support on the HRMS experiments. The Acknowledgements were updated on November 5, 2014.

Received: May 25, 2014
Published online: August 26, 2014

[1] http://www.heliatek.com/newscenter/latest_news/neuer-weltrekord-fur-organische-solarzellen-heliatek-behauptet-sich-mit-12-zell-effizienz-als-technologiefuhrer/?lang=en (accessed: May 2014).
[2] F. C. Krebs, N. Espinosa, M. Hösel, R. R. Søndergaard, M. Jørgensen, *Adv. Mater.* **2014**, *26*, 29–39.
[3] a) Z. C. He, H. B. Wu, Y. Cao, *Adv. Mater.* **2014**, *26*, 1006–1024; b) T. H. Lai, S. W. Tsang, J. R. Manders, S. Chen, F. So, *Mater. Today* **2013**, *16*, 424–432.
[4] a) S. E. Shaheen, C. J. Brabec, N. S. Sariciftci, F. Padinger, T. Fromherz, J. C. Hummelen, *Appl. Phys. Lett.* **2001**, *78*, 841–843; b) K. Zilberberg, J. Meyer, T. Riedl, *J. Mater. Chem. C* **2013**, *1*, 4796–4815.
[5] a) P. Peumans, A. Yakimov, S. R. Forrest, *J. Appl. Phys.* **2003**, *93*, 3693–3723; b) A. W. Hains, Z. Q. Liang, M. A. Woodhouse, B. A. Gregg, *Chem. Rev.* **2010**,*110*, 6689–6735.
[6] a) T. V. Pho, H. Kim, J. H. Seo, A. J. Heeger, F. Wudl, *Adv. Funct. Mater.* **2011**, *21*, 4338–4341; b) K. Sun, B. M. Zhao, V. Murugesan, A. Kumar, K. Y. Zeng, J. Subbiah, W. W. H. Wong, D. J. Jones, J. Y. Ouyang, *J. Mater. Chem.* **2012**, *22*, 24155–24165; c) K. M. O'Malley, C. Z. Li, H. L. Yip, A. K. Y. Jen, *Adv. Energy Mater.* **2012**, *2*, 82–86.
[7] Y. Zhou, C. Fuentes-Hernandez, J. Shim, J. Meyer, A. J. Giordano, H. Li, P. Winget, T. Papadopoulos, H. Cheun, J. Kim, M. Fenoll, W. Haske, E. Najafabadi, S. Barlow, J. L. Brédas, S. R. Marder, A. Kahn, B. Kippelen, *Science* **2012**, *336*, 327–332.
[8] a) P. Peumans, V. Bulović, S. R. Forrest, *Appl. Phys. Lett.* **2000**, *76*, 2650–2652; b) H. Gommans, B. Verreet, B. P. Rand, R. Muller, J. Poortmans, P. Heremans, J. Genoe, *Adv. Funct. Mater.* **2008**, *18*, 3686–3691; c) G. Chen, H. Sasabe, Z. Q. Wang, X. F. Wang, Z. R. Hong, Y. Yang, J. Kido, *Adv. Mater.* **2012**, *24*, 2768–2773; d) Y. Zhou, T. Taima, T. Kuwabara, K. Takahashi, *Adv. Mater.* **2013**, *25*, 6069–6075.
[9] Q. L. Song, F. Y. Li, H. Yang, H. R. Wu, X. Z. Wang, W. Zhou, J. M. Zhao, X. M. Ding, C. H. Huang, X. Y. Hou, *Chem. Phys. Lett.* **2005**, *416*, 42–46.
[10] a) S. W. Liu, C. C. Lee, C. F. Lin, J. C. Huang, C. T. Chen, J. H. Lee, *J. Mater. Chem.* **2010**, *20*, 7800–7806; b) S. H. Liao, J. R. Shiu, S. W. Liu, S. J. Yeh, Y. H. Chen, C. T. Chen, T. J. Chow, C. I. Wu, *J. Am. Chem. Soc.* **2009**, *131*, 763–777.
[11] a) M. Y. Chan, C. S. Lee, S. L. Lai, M. K. Fung, F. L. Wong, H. Y. Sun, K. M. Lau, S. T. Lee, *J. Appl. Phys.* **2006**, *100*, 094506; b) V. Steinmann, N. M. Kronenberg, M. R. Lenze, S. M. Graf, D. Hertel, K. Meerholz, H. Bürckstümmer, E. V. Tulyakova, F. Würthner, *Adv. Energy Mater.* **2011**, *1*, 888–893.
[12] C. Li, M. Schwab, Y. F. Zhao, L. Chen, I. Bruder, I. Münster, P. Erk, K. Müllen, *Dyes Pigm.* **2013**, *97*, 258–261.
[13] a) K. S. Yook, S. O. Jeon, O. Y. Kim, J. Y. Lee, *Electrochem. Solid-State Lett.* **2011**, *14*, B59–B62; b) H. W. Li, C. W. Lu, L. Y. Lin, Y. H. Chen, W. C. Lin, K. T. Wong, F. Lin, *J. Mater. Chem. A* **2013**, *1*, 1770–1777; c) S. J. Su, T. Chiba, T. Takeda, J. Kido, *Adv. Mater.* **2008**, *20*, 2125–2130.
[14] J. J. You, M. F. Lo, W. M. Liu, T. W. Ng, S. L. Lai, P. F. Wang, C. S. Lee, *J. Mater. Chem.* **2012**, *22*, 5107–5113.
[15] C. Falkenberg, C. Uhrich, S. Olthof, B. Maennig, M. K. Riede, K. Leo, *J. Appl. Phys.* **2008**, *104*, 034506.
[16] J. S. Yu, N. N. Wang, Y. Zang, Y. D. Jiang, *Sol. Energy Mater. Sol. Cells* **2011**, *95*, 664–668.
[17] A. Bencini, V. Lippolis, *Coord. Chem. Rev.* **2010**, *254*, 2096–2180.
[18] a) S. H. Oh, S. I. Na, J. Jo, B. Lim, D. Vak, D. Y. Kim, *Adv. Funct. Mater.* **2010**, *20*, 1977–1983; b) C. H. Wu, C. Y. Chin, T. Y. Chen, S. N. Hsieh, C. H. Lee, T. F. Guo, A. K. Y. Jen, T. C. Wen, *J. Mater. Chem. A* **2013**, *1*, 2582–2587; c) S. O. Jeon, J. H. Kim, J. W. Kim, Y. Park, J. Y. Lee, *J. Phys. Chem. C* **2011**, *115*, 18789–18794; d) J. Liu, Y. H. Xue, Y. X. Gao, D. S. Yu, M. Durstock, L. M. Dai, *Adv. Mater.* **2012**, *24*, 2228–2233.
[19] Y. Y. Liang, Z. Xu, J. B. Xia, S. T. Tsai, Y. Wu, G. Li, C. Ray, L. P. Yu, *Adv. Mater.* **2010**, *22*, E135–E138.
[20] K. Vandewal, K. Tvingstedt, A. Gadisa, O. Ingnäs, J. V. Manca, *Nat. Mater.* **2009**, *8*, 904–909.
[21] a) B. Y. Qi, J. Z. Wang, *J. Mater. Chem.* **2012**, *22*, 24315–24325; b) B. Y. Qi, J. Z. Wang, *Phys. Chem. Chem. Phys.* **2013**, *15*, 8972–8982.
[22] M. D. Bhatt, S. Suzuki, T. Sakurai, K. Akimoto, *Appl. Surf. Sci.* **2010**, *256*, 2661–2667.
[23] S. Zhong, R. Wang, H. Y. Mao, Z. C. He, H. B. Wu, W. Chen, Y. Cao, *J. Appl. Phys.* **2013**, *114*, 113709.
[24] a) Z.-C. He, C.-M. Zhong, X. Huang, W.-Y. Wong, H.-B. Wu, L.-W. Chen, S.-J. Su, Y. Cao, *Adv. Mater.* **2011**, *23*, 4636–4643; b) C.-H Duan, K. Zhang, X. Guan, C.-M. Zhong, H.-M. Xie, F. Huang, J.-W. Chen, J. B. Peng, Y. Cao, *Chem. Sci.* **2013**, *4*, 1298–1307.
[25] S. Naka, H. Okada, H. Onnagawa, *Appl. Phys. Lett.* **2000**, *76*, 197–199.